THE JOURNAL OF BIOLOGICAL CHEMISTRY
Vol. 280, No. 17, Issue of April 29, pp. 17076–17083, 2005
Printed in U.S.A.

Regulation of Poly(ADP-ribose) Polymerase-1 by DNA Structure-specific Binding*[S]

Received for publication, November 30, 2004, and in revised form, February 8, 2005
Published, JBC Papers in Press, February 28, 2005, DOI 10.1074/jbc.M413483200

Irina Lonskaya‡, Vladimir N. Potaman§, Luda S. Shlyakhtenko¶, Elena A. Oussatcheva§, Yuri L. Lyubchenko¶, and Viatcheslav A. Soldatenkov‡‖

From the ‡Department of Radiation Medicine, Lombardi Comprehensive Cancer Center, Georgetown University Medical Center, Washington, D. C. 20057, the §Institute of Biosciences and Technology, The Texas A&M University System Health Science Center, Houston, Texas 77030, and the ¶Department of Pharmaceutical Sciences, University of Nebraska Medical Center, Omaha, Nebraska 68198

Poly(ADP-ribose) polymerase-1 (PARP-1) is an intracellular sensor of DNA strand breaks and plays a critical role in cellular responses to DNA damage. In normally functioning cells, PARP-1 enzymatic activity has been linked to the alterations in chromatin structure associated with gene expression. However, the molecular determinants for PARP-1 recruitment to specific sites in chromatin in the absence of DNA strand breaks remain obscure. Using gel shift and enzymatic footprinting assays and atomic force microscopy, we show that PARP-1 recognizes distortions in the DNA helical backbone and that it binds to three- and four-way junctions as well as to stably unpaired regions in double-stranded DNA. PARP-1 interactions with non-B DNA structures are functional and lead to its catalytic activation. DNA hairpins, cruciforms, and stably unpaired regions are all effective co-activators of PARP-1 auto-modification and poly(ADP-ribosyl)ation of histone H1 in the absence of free DNA ends. Enzyme kinetic analyses revealed that the structural features of non-B form DNA co-factors are important for PARP-1 catalysis activated by undamaged DNA. $K_{0.5}$ constants for DNA co-factors, which are structurally different in the degree of base pairing and spatial DNA organization, follow the order: cruciform ≤ hairpin ≪ loop. DNA structure also influenced the reaction rate; when a hairpin was substituted with a stably unpaired region, the maximum reaction velocity decreased almost 2-fold. These data suggest a link between PARP-1 binding to non-B DNA structures in genome and its function in the dynamics of local modulation of chromatin structure in the normal physiology of the cell.

Poly(ADP-ribose) polymerization is a post-translation protein modification that utilizes an ADP-ribosyl moiety from NAD^+ to form branched polymers of up to 200 ADP-ribose units, which are attached via glutamic acid residues to the nuclear acceptor proteins. The best understood member of the superfamily of poly(ADP-ribose) polymerases (1) is PARP-1,[1] whose activity is largely accounted for by this type of nuclear protein modification (2). PARP-1 is an abundant zinc finger-containing nuclear protein present at ~1 enzyme/50 nucleosomes. It has high affinity for damaged DNA and becomes catalytically active upon binding to double- and single-stranded DNA breaks (3). PARP-1 activation leads to modification of nuclear proteins including itself (auto-modification reaction) with a very strong polyanion, poly(ADP-ribose). This modification has a profound effect on the structure and function of the acceptor proteins. Based on these properties, PARP-1 has long been regarded as an intracellular sensor of DNA strand breaks, and its function has been considered in context with the cellular responses to genotoxic stress, in particular DNA damage repair and apoptosis (4–7).

In undamaged cells, recruitment of PARP-1 to the chromatin-modifying complex leads to a dramatic and localized perturbation of histone-DNA contacts (8, 9), allowing DNA to be accessible to regulatory factors, thus implicating PARP-1 in fundamental processes, such as DNA replication, recombination, and transcription (reviewed in Ref. 10). Recently, PARP-1 enzymatic activity has been linked to the coordination of chromatin structure and gene expression in *Drosophila* (11) and to the post-translational modification of chromatin insulators (12). Several lines of evidence indicate that PARP-1 may exert its function in transcription through (i) direct binding to gene-regulating sequences, (ii) modulation of the nucleoprotein architecture of chromatin, or (iii) modification of transcription factors by poly(ADP-ribosyl)ation (reviewed in Refs. 13 and 14). However, the molecular determinants for PARP-1 recruitment to the specific chromatin sites in normally functioning cells (in the absence of genotoxic stress) remain obscure. Furthermore, the dependence of PARP-1 function on the presence of strand breaks in DNA provides no clue to a mechanism by which it may ADP-ribosylate transcription regulators and structural chromatin proteins in the absence of DNA damage. One possibility is suggested from PARP-1 activation following its binding to non-B DNA structures, such as hairpins, cruciforms, and unwound regions that can form in the transcriptional regulatory elements, many of which contain palindromic or AT-rich sequences (15–17). In support of this suggestion, reports from several laboratories presented evidence of PARP-1 interactions with local non-B DNA structures containing partially unwound sequences and with base-unpaired region within the matrix attachment regions of eukaryotic genomic DNA (18–22). It is conceivable that these interactions are functional and may stimulate the catalytic activation of PARP-1. Subsequent ADP-

* This work was supported in part by National Institutes of Health Grants CA74175-07 and GM62235. The costs of publication of this article were defrayed in part by the payment of page charges. This article must therefore be hereby marked "*advertisement*" in accordance with 18 U.S.C. Section 1734 solely to indicate this fact.

[S] The on-line version of this article (available at http://www.jbc.org) contains a supplemental table.

‖ To whom correspondence should be addressed: Dept. of Radiation Medicine, Lombardi Comprehensive Cancer Center, Georgetown University Medical Center, 3970 Reservoir Rd., N.W., The Research Bldg., Rm. E-204A, Box 571482, Washington, D. C. 20057-1482. Fax: 202-687-0400; E-mail: soldates@georgetown.edu.

[1] The abbreviations used are: PARP-1, poly(ADP-ribose) polymerase-1; PAR, poly(ADP-ribose) polymer; dsDNA, double-stranded DNA; AFM, atomic force microscopy.

ribosylation of histones and nonhistone proteins at PARP-1-binding sites may result in transient and local chromatin loosening, thus alleviating nucleosomal repression of transcription (11).

In this work we have investigated two aspects of PARP-1 operational properties that may shed light on its function in the dynamics of chromatin structure: its ability to interact with undamaged DNA in a structure-specific fashion and its enzymatic activation upon binding to non-B DNA structures that can form in genomic DNA. Using various types of DNA substrates with defined structures, we show that DNA hairpins, cruciforms, and stably unpaired regions are all effective co-enzymatic activators of PARP-1 auto-modification and poly-(ADP-ribosyl)ation of histone H1 in the absence of free DNA ends. Furthermore, we demonstrate that the co-factor efficiency of DNA depends on the structural properties of the PARP-1-binding site. These observations provide a rational basis for understanding PARP-1 function as a component of a chromatin-modifying complex and its role as a transcriptional regulator in normal cell physiology.

EXPERIMENTAL PROCEDURES

DNA Constructs—Plasmids pDT20, pEO30HE, pUC8S3B, pUC8S1F2, and pUC8F14C containing 20-, 30-, 42-, 60-, and 106-bp inverted repeat inserts, respectively, have been described (23). To create plasmid pMDR1S, the 14-bp sequence between the BamHI and HindIII sites of pUC8 vector was replaced with the sequence AAGAAGGAAAAGAA. The sequences of the inserts are available as on-line supplementary material. The 301-bp fragments of pUC8 and similar fragments of insert-containing plasmids were amplified using upstream (5′-biotin-CTGGCACGACAGGTTTCCCGACTG-3′) and downstream (5′-biotin-CTGGCGAAAGGGGGATGTGCTGCA-3′) modified PCR primers (Sigma-Genosys, The Woodlands, TX) hybridizing at the two PvuII sites. Subsequent pairwise hybridization of the PvuII-PvuII fragments produced heteroduplexes with three-way junctions (pUC8 × pEO30HE) and (pUC8 × pDT20), a four-way junction (pEO30HE × pDT20), and a 14-bp loop (pUC8 × pMDR1S). In some experiments, fragments of pUC8 were amplified using one biotinylated (upstream) and another unmodified (downstream) primer, resulting in a linear DNA duplex with a biotin group at only one end.

DNA Heteroduplex Formation and Isolation—DNA strands containing 5′-biotin groups were annealed with their complementary counterparts to form heteroduplexes, as described (23) with minor modifications (Fig. 1). Briefly, a 25-μl hybridization mixture containing 1 pmol of each DNA fragment in 200 mM NaCl, 50 mM Tris-HCl, pH 8.0, 1 mM dithiothreitol, 10 mM $MgCl_2$ was incubated stepwise at 95 °C (5 min), 85 °C (10 min), and 70 °C (60 min) and then cooled to room temperature. The hybridization products were separated in a 5% native polyacrylamide gel in TBE buffer (90 mM Tris borate, pH 8.3, 2.5 mM EDTA), and bands of heteroduplex fragments that migrate slower than correctly annealed parental fragments were excised. After purification using a GeneClean gel extraction kit (Qbiogen, Carlsbad, CA), isolated heteroduplexes were resuspended in 40 μl of TE (10 mM Tris-HCl, 1 mM EDTA, pH 7.8), and aliquots were taken for the PARP-1 binding reactions and activity assays. The cruciform heteroduplex construct (pEO30HE × pUC8S3B) for enzymatic footprinting was prepared as described above, except that, during the PCR, the ^{32}P-radiolabeled primers were used instead of the biotin-labeled ones. For AFM imaging, stable cruciforms carrying 30- and 53-bp hairpins were generated from the PvuII-PvuII restriction fragments of plasmids pUC8S1F2 and pUC8F14C, which were hybridized and purified as described above.

PARP-1 Binding Reactions—PARP-1 binding assays were carried out in the presence of recombinant full-length human PARP-1 (specific activity 10 units/μg; Trevigen, Gaithersburg, MD) at varying DNA-protein molar ratios (indicated in the figure legends) in a buffer containing 12.5 mM HEPES, pH 7.9, 15 mM $MgCl_2$, 0.5 mM EDTA, 50 mM KCl, 2 mM β-mercaptoethanol, 0.05% Nonidet P-40, and 7.5% glycerol. DNA constructs were modified by binding a streptavidin-alkaline phosphatase conjugate (Vector Laboratories, Burlingame, CA) to the biotinylated DNA ends according to the manufacturer's protocol. This modification prevents PARP-1 binding to the DNA ends and allows post-EMSA DNA visualization using DuoLux chemiluminescent substrate (UltraSNAP detection system; Vector Laboratories). Linear DNA homoduplexes with one unprotected end were used as positive controls for PARP-1 binding to blunt DNA ends, whereas the 301-bp fragments of pUC8 with two protected ends were used as negative controls for nonspecific PARP-1 binding in these experiments. All of the binding reactions (total volume 30 μl) containing equimolar amounts of DNA probe (1.7 nM) and varying amounts of protein were for 15 min at 25 °C. The reaction products were loaded on 3.5% native polyacrylamide gels containing 5% glycerol and separated by electrophoresis at 200 V in TBE buffer for 2.5 h. The gels were then soaked in 0.5 × TBE buffer for 15 min at room temperature, and DNA-protein complexes were transferred to a positively charged nitrocellulose membrane Hybond-N+ (Amersham Biosciences) using a semi-dry trans-blot SD apparatus (Bio-Rad). Transferred DNA was cross-linked to the membrane at 120 mJ/cm^2 using a Stratalinker UV-Crosslinker (Stratagene, La Jolla, CA) and visualized using an Ultra Snap detection kit (Vector Laboratories) as suggested by the manufacturer. Densitometry of the films was performed using ImageQuant 5.0 software, (Molecular Dynamics, Sunnyvale, CA). DNA migration in the gels was measured as the distance (mm) between the half-height of the band front and the start point, and the relative gel mobility was calculated as $r = DNA_{PARP}/DNA_0$, where DNA_0 and DNA_{PARP} are the migration distances of DNA constructs in the absence and the presence of varying concentration of PARP-1.

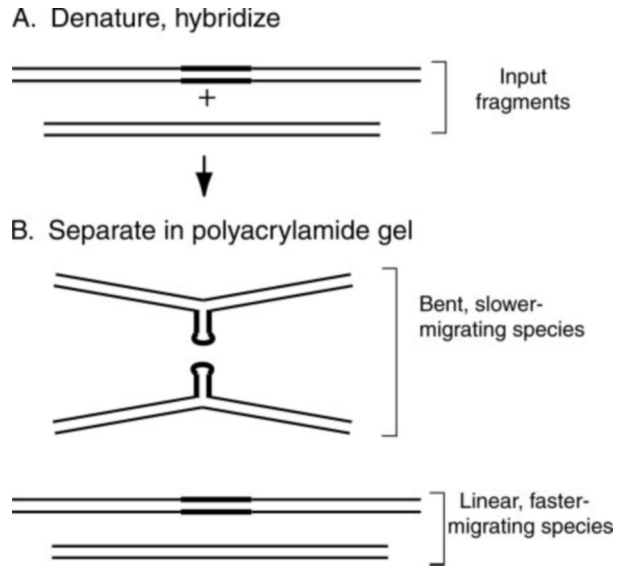

FIG. 1. **Schematics of heteroduplex DNA preparation.** Hybridization of two DNA fragments that are complementary everywhere except the non-B DNA forming regions by denaturation-renaturation results in four DNA molecules. The two linear DNAs identical to the initial fragments migrate in a polyacrylamide gel according to their molecular weights. The two heteroduplex fragments are usually bent at the junctions between the duplex and secondary structures, migrate slower, and can therefore be separated from the linear fragments.

PARP-1 Footprinting—To saturate binding sites for footprinting, we used a 50-fold molar excess of PARP-1 over the heteroduplex DNA substrate. Protein binding was performed for 10 min on ice in a volume of 25 μl containing 4 nM heteroduplex substrate and 200 nM PARP-1 in the binding buffer (25 mM Tris-HCl, pH 8.0, 50 mM KCl, 6.25 mM $MgCl_2$, 0.5 mM dithiothreitol, 10% glycerol) from the Core Footprinting System kit (Promega, Madison, WI). For DNase I reactions, the binding mixtures were supplemented with 25 μl of a mixture of 5 mM $CaCl_2$ and 10 mM $MgCl_2$ and incubated for 1 min at room temperature, and then 3 μl (0.3 units) of DNase I (Promega) were added. After 2 min of incubation at room temperature, the DNase I reactions were terminated by the addition of 45 μl of stop solution (200 mM NaCl, 30 mM EDTA, 1% SDS, 100 μg/ml yeast tRNA); the samples were extracted with phenol and chloroform; and DNA was precipitated with ethanol. Control samples lacking PARP-1 were treated identically to the binding mixtures. Footprinting with P1 nuclease (United States Biochemical, Cleveland, OH) was accomplished by adding 2 μl (2 units) of the enzyme to the binding mixtures, and incubation was continued for 4 min on ice, followed by immediate phenol and chloroform extraction and ethanol precipitation. The enzyme-treated DNA was analyzed in a 7% denaturing polyacrylamide gel using products of DNA sequencing reactions as markers.

Sample Preparation and Imaging with AFM—To visualize PARP-1/heteroduplex DNA complexes, binding reactions were performed for 10

min on ice in a volume of 10 μl containing 0.5 pmol of heteroduplex substrate and 15 pmol of PARP-1 in the binding buffer (40 mM HEPES, pH 7.4, 100 mM NaCl, 10 mM $MgCl_2$). The protein was then cross-linked to DNA with 0.8% glutaraldehyde for 15 min, and the reaction was terminated by the addition of 5 μl of 2 M Tris-HCl, pH 7.7. After the removal of unbound protein using G-25 spin columns, protein-DNA complexes were diluted 10-fold with 10 mM HEPES, pH 7.4, placed onto aminopropyl silatrane-modified mica for 2 min, rinsed with deionized water, and dried with argon as described (24). The images were acquired in air with a MultiMode SPM NanoScope IIIa system using tapping mode etched silicon probes (Veeco/Digital Instruments, Santa Barbara, CA). The images were processed, and the measurements were performed with Femtoscan software, version 1.6 (Advanced Technologies Center, Moscow, Russia). For statistics, 100–120 uncomplexed DNA molecules and no less than 50 unobstructed PARP-DNA complexes with each type of DNA template were analyzed. The data shown are the means ± standard deviation of the mean.

Trans-poly (ADP-ribosyl)ation of Histone H1—Trans-ADP-ribosylation of histone H1 (Roche Applied Science) was measured using a colorimetric assay (Trevigen) for incorporation of biotinylated NAD (6-biotin-17-nicotinamide-adenine-dinucleotide) in a poly(ADP-ribose) polymer (PAR) primed at solid phase immobilized histone H1 as suggested by the manufacturer. All of the kinetic measurements were carried out in a 96-well plate in a solution of 100 mM Tris-HCl (pH 8.0), 50 mM NaCl, 5 mM $MgCl_2$, 2 mM β-mercaptoethanol, 0.5 mM EDTA in the presence of 400 μM NAD^+ (Sigma) supplemented with 50 μM biotinylated NAD^+ (Trevigen) and increasing concentrations of DNA (0–100 pM) as a co-factor. ADP-ribosylation reactions were initiated by addition of purified PARP-1 protein at varying concentrations, as indicated in the legends to Figs. 6 and 7. The reactions (50 μl volume) were carried out for 30 min at 25 °C and terminated by decanting the reactant solution, and histone H1 coats were washed four times with 100 μl of phosphate-buffered saline/well. Biotinylated PAR attached to histone H1 layered on the surface of a microwell plate was quantified using a streptavidin-horseradish peroxidase system and the TACS Sapphire substrate (Trevigen). The reaction rates (V) were calculated from the chromogen absorbance at 620 nm using a Labsystems Multiscan Accent plate reader and software version 2.4.1 (Woburn, MA) and expressed in relative units as described (25). In the presence of hairpin-containing DNA co-factor, the reaction rates increased in a time-dependent fashion and did not reach steady-state levels by 30 min of incubation at 25 °C. To calculate the $K_{0.5}$ and V_{max} values for the poly(ADP-ribosyl)ation reactions from the kinetic curves using nonlinear regression fits, the kinetic data were fit by the equation $y = a^*x^b/(c^b + x^b)$, where $a = V_{max}$; b is an empirical measure of the curve steepness; and c corresponds to the DNA concentration at $V_{max}/2$, and were expressed as $K_{0.5}$. Goodness of the fit was assessed by the coefficient of determination (R^2), and the statistical analysis for significance of kinetic parameters was performed using SigmaPlot 2000 software. Each value is the average of three independent experiments, and standard deviations are estimated at ± 5% of the mean.

Auto-poly(ADP-ribosyl)ation of PARP-1—The reactions were carried out in the same buffer as used in the trans-poly(ADP ribosyl)ation assay in the presence of 450 μM NAD^+ (Sigma) and different types of dsDNA co-factors added at a concentration of 1.7 nM. ADP-ribosylation was induced by the addition of purified PARP-1 to a final protein concentration of 14.3 nM, and the reaction mixture was incubated at 25 °C for 30 min. The reaction was terminated by adding 2× SDS-PAGE loading buffer, and the samples were heated at 100 °C for 5 min and resolved by SDS-PAGE in a 4–12% gradient bis-Tris gel (NuPAGE; Invitrogen). *In vitro* auto-modified PARP-1 (Biomol, Plymouth Meeting, PA) was loaded onto the gel (50 ng/lane) alongside the reaction samples as an immunoblotting standard. The extent of PARP-1 auto-poly(ADP-ribosyl)ation was determined by Western blot analysis with a mouse monoclonal anti-poly(ADP-ribose) antibody (1:500, Biomol). Equal sample loading was verified by reprobing the same blots with mouse anti-PARP antibody (1:500, clone 42; BD Transduction Labs, Lexington, KY). The signals were detected using an enhanced chemiluminescence system (Amersham Biosciences).

RESULTS AND DISCUSSION

Macromolecular Association of PARP-1 Protein with Duplex DNA in the Absence of Free DNA Ends—Local non-B DNA structures are generally not thermodynamically stable in linear DNA fragments (26). Therefore, to investigate DNA structure-specific PARP-1 binding activity, we generated a reference set of DNA heteroduplexes containing stably formed loop and stem-loop structures based on a 301-bp PvuII-PvuII fragment of pUC8 (23). The heteroduplex parts of the constructs contained (Table I): (a) a 15-bp hairpin (three-way junction), (b) a 10-bp hairpin (three-way junction), (c) a cruciform (four-way junction) with 10- and 15-bp arms, and (d) a 14-bp loop (loopout region). Because the presence of free DNA ends may interfere with PARP-1 binding to non-B DNA structures, the constructs were modified by binding streptavidin to the biotinylated DNA ends (27). The end-protected parental DNA homoduplex was utilized as a negative control for protein binding to the linear parts of DNA heteroduplexes.

TABLE I
Structural features of double-stranded DNA constructs used in PARP-1 binding and activity assays

The cartoons on the left depict structural characteristic of dsDNA constructs modified with streptavidin (filled oval) coupled to 5′-biotinylated DNA ends.

	DNA duplex	Ends modified	Insert type	Insert Size, bp
a	pUC8/pEO30HE	two	hairpin	30
b	pUC8/pDT20p	two	hairpin	20
c	pEO30HE/pDT20	two	cruciform	30/20
d	pUC8/pMDR1S	two	loop	14
e	pUC8/pUC8	two	none	none
f	pUC8/pUC8	one	none	none

PARP-1 binding to the distinct types of non-B DNA structures such as loops, hairpins, and cruciforms was assayed over a range of protein concentrations under noncatalytic conditions, that is, in the absence of NAD^+. PAGE analysis (Fig. 2) shows that PARP-1 binding to end-protected DNA heteroduplexes resulted in complexes with progressively retarded mobility at increasing protein concentrations. In contrast, the gel mobility of the end-protected parental DNA homoduplex was not affected by PARP-1, ruling out its affinity for sequences in the linear parts of heteroduplexes. It should be noted that the modification of DNA ends with two molecules of streptavidin-alkaline phosphatase conjugate yielded a DNA-protein complex (an estimated molecular mass of 490 kDa) with predictably slow gel mobility. This resulted in a small separation between the PARP-1-bound and unbound DNA-streptavidin complexes. Similar small changes in mobility have been observed for PARP-1 complexes with 300-bp DNA mini-circles (21) or streptavidin-bound linear DNA oligonucleotides containing a Tax-responsive element (28). The estimated K_d values for PARP-1 binding to non-B DNA structures are in the low nanomolar range, which is comparable with PARP-1 affinity for AT-rich sequences in the matrix attachment regions (21) and for the Tax-responsive element (28) in undamaged DNA.

To visualize PARP-1 binding to non-B DNA structures we employed AFM, which allows simultaneous visualization at nanometer resolution of PARP-1 binding to different sites in a DNA molecule such as DNA ends and structural alterations in dsDNA. Previously, we utilized AFM to demonstrate specific interactions between PARP-1 and hairpin-containing dsDNA (22). Fig. 3 shows that PARP-1 binds to the free DNA ends (positive control for DNA binding activity) as well as to internal sites corresponding to the positions of the four-way junction or stably unpaired region in DNA heteroduplexes. In DNA constructs used in this study, the distance between the site of the non-B DNA structure and the nearest end was about 40% of the total heteroduplex fragment length. Following PARP-1 binding, the distances of the internal PARP-1 binding sites from the fragment ends were measured and were expressed as percent-

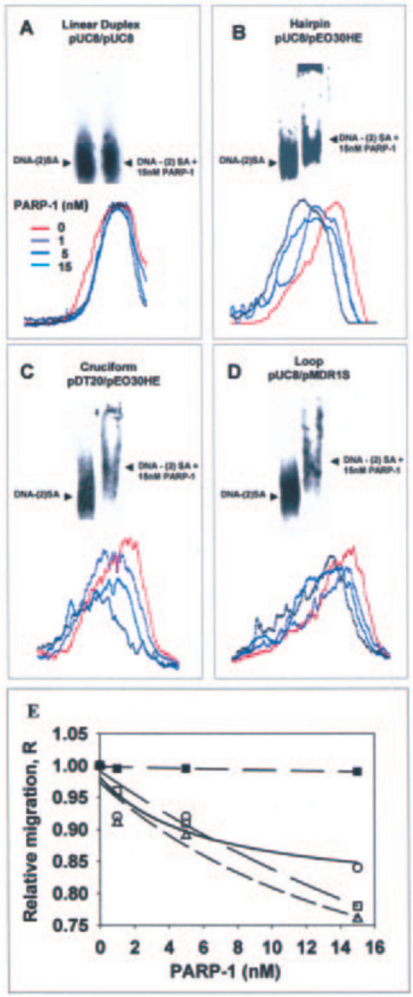

FIG. 2. **PARP-1 forms macromolecular complexes with loop and stem-loop DNA structures in the absence of free DNA ends.** Linear dsDNA fragments (*A*) and DNA heteroduplexes containing a stably formed hairpin (*B*), a cruciform (*C*), or a loop (*D*) blocked at both ends with molecules of streptavidin (*(2) SA*) were incubated with increasing concentrations of PARP-1 under noncatalytic conditions. Equimolar amounts of DNA (1.7 nM) were used in all binding reactions. *A–D*, *top panels*, unbound DNA and DNA-protein complexes were subjected to nondenaturing PAGE and blotted onto nitrocellulose membrane, and DNA was visualized using an Ultra Snap detection kit. *A–D*, *bottom panels*, gel mobilities of DNA-(2) SA-PARP-1 complexes were analyzed using the ImageQuant software. *E*, the relative gel mobilities of bound and unbound DNAs were quantified from gel scans shown in *A–D* as described under "Experimental Procedures" and plotted against the PARP-1 concentration. The end-protected heteroduplexes contained a hairpin (○), a cruciform (□), or a loop (△). Linear DNA homoduplexes (■) were modified with streptavidin at both DNA ends.

ages of the total fragment length. The distances between bound PARP-1 and the closest end were 37.5 ± 3.0% and 38.5 ± 4.5% for DNA constructs containing unpaired loops and immobile cruciforms, respectively. These data are within an error range expected for the location of the non-B DNA structures in the heteroduplexes. Importantly, no other internally located DNA-protein complexes were observed in the heteroduplex fragments, which rules out nonspecific or sequence-specific PARP-1 binding to B DNA.

Additional and more crucial evidence of targeted PARP-1 binding to the non-B DNA sites comes from nuclease mapping of the protein binding sites at cruciforms in DNA (Fig. 4). The PARP-1 complex with the heteroduplex fragment containing the stable cruciform formed by the nonidentical inverted repeats was probed with DNase I that digests double-stranded DNA and P1 nuclease that digests single-stranded DNA. Fig. 4*A* shows PARP-1-dependent sites in the DNase I digestion pattern that map to the internucleotide linkages in the vicinity of the hairpin tip; PARP-1 protects DNase I-susceptible sites in both strands adjacent to the tip. Nuclease P1 reactivity toward the single-stranded loop of the hairpin is also inhibited by PARP-1 binding. The nucleotide resolution footprinting results (Fig. 4) show that PARP-1 binds near the stem-loop boundaries in the cruciform hairpins and does not appreciably bind to linear double-stranded DNA in other parts of the heteroduplex. Similarly, in the case of the loop-containing heteroduplex fragment, PARP-1 may recognize and bind to the double/single-stranded boundary.

Taken together, the gel shift, AFM, and footprinting data (Figs. 2–4) are consistent with the previously reported observations that PARP-1 may bind DNA in a structure-specific manner regardless of the absence or the presence of free DNA ends (reviewed in Ref. 14). Several laboratories have shown that PARP-1 has a preference for supercoiled DNA compared with a relaxed template (18) and binds to hairpins and cruciform structures in duplex DNA (19, 22) and to the DNA unwound regions (21). From our data (Figs. 2–4), it appears that PARP-1 has a relatively high affinity for non-B DNA structures, allowing its binding to DNA secondary structures in the presence of free DNA ends as competitors. Although the molecular basis for the PARP-1-non-B DNA interactions requires further investigation, it is likely that PARP-1 recognition and binding to non-B DNA structures in genomic DNA has functional significance, *e.g.* for modulation of the chromatin structure. This suggestion is in line with previous reports implicating PARP-1 in chromatin structural transitions in the absence of genotoxic stress (reviewed in Ref. 10).

Stem-Loop DNA Constructs Stimulate Auto-poly(ADP-ribosyl)ation of PARP-1—The requirement of DNA containing strand breaks as a co-factor stimulating the enzymatic activity of PARP-1 is well established (3). PARP-1 binding to single- or double-stranded breaks in DNA results in a burst of covalent poly(ADP-ribosyl)ation of PARP-1 itself or other nuclear acceptor proteins in reactions defined as auto- or trans-ADP-ribosylation, respectively (reviewed in Refs. 4 and 29). The above described ability of PARP-1 to form macromolecular complexes with DNA in a structure-specific fashion prompted us to investigate whether such physical interactions result in the catalytic activation of PARP-1. To address this question, we evaluated the auto-poly(ADP-ribosyl)ation rates upon PARP-1 binding to non-B DNA structures under conditions optimal for catalytic activity of mammalian PARP-1 proteins and with NAD^+ at an upper limit of physiological concentrations (30). The *in vitro* auto-poly(ADP-ribosyl)ation of PARP-1 was stimulated by the addition of different non-B DNA constructs (Fig. 5*A*, *lanes 2–5*) or fragmented DNA (Fig. 5*A*, *lanes 6* and *7*), and the extent of PARP-1 auto-modification was evaluated by an immunoblotting assay using antibodies raised against PAR. As expected, randomly fragmented DNA effectively stimulated the ADP-ribosyltransferase activity of PARP-1, resulting in the synthesis of a heterogeneous ADP-ribose polymer (Fig. 5*A*, *lane 7*). Linear dsDNA with the ends protected with streptavidin did not interact with PARP-1 in the binding assays (Fig. 2) and exhibited no potential to stimulate PARP-1 catalytic activity (Fig. 5*A*, *lane 1*). Importantly, each DNA construct carrying a single recognition site for PARP-1 binding, such as an unprotected blunt end (*lane 6*), hairpins (*lanes 3* and *5*), a cruciform (*lane 4*), or a loop (*lane 2*) markedly enhanced PARP-1 auto-poly(ADP-ribosyl)ation over a basal level (*lane 1*) (Fig. 5). These data indicate that non-B DNA structures are potent co-factors of PARP-1, thus suggesting functional importance of DNA structure-specific PARP-1 binding.

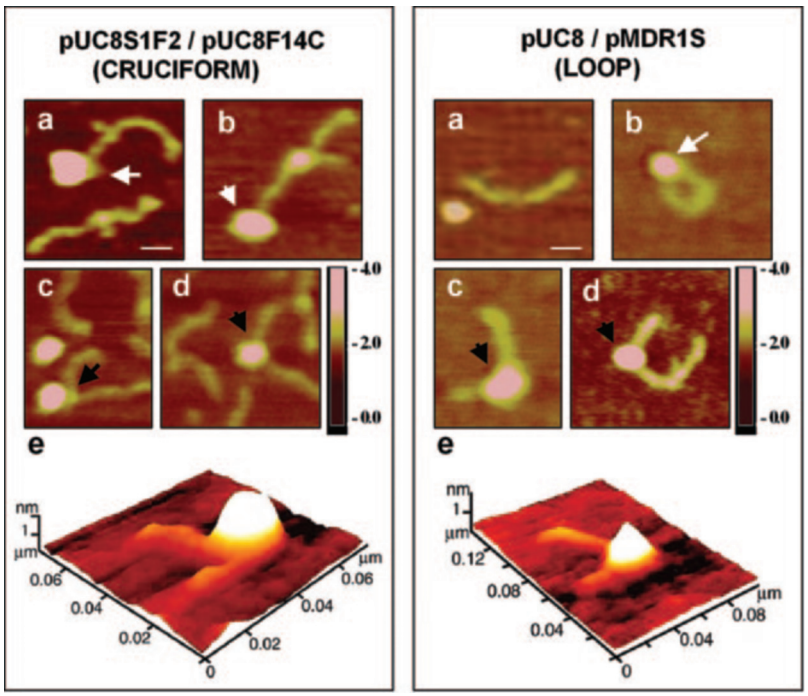

FIG. 3. **AFM imaging of PARP-1 binding to non-B DNA structures.** DNA heteroduplexes carrying a cruciform (*left panels*) or stably unpaired regions (*right panels*) were incubated with PARP-1 as described under "Experimental Procedures," and the reaction products were visualized by AFM. Representative AFM images of free DNA molecules (*a*) and the PARP-1 protein-DNA heteroduplex complexes (*a–e*) are shown. *White* and *black arrows* indicate end-bound (*a* and *b*) and internally bound (*c* and *d*) PARP-1 molecules, respectively. The three-dimensional representations of the PARP-1-DNA complexes are shown in *panel e*. The *scale bars* represent 25 nm. The *color-coded bar* on the right indicates the height scale and corresponds to a 0.0–4.0 nm range (from *dark* to *bright*).

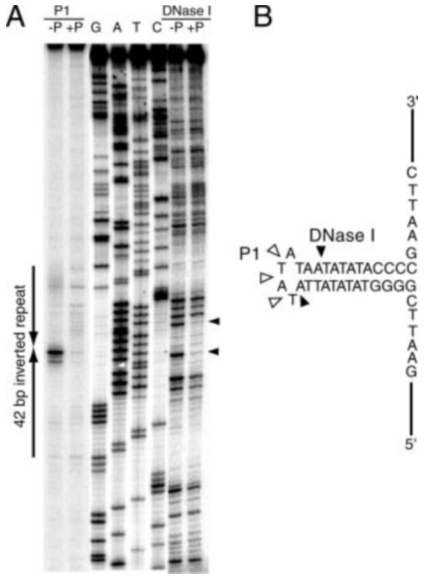

FIG. 4. **Nuclease footprinting of a stable DNA cruciform.** The cruciform substrate was formed with two nonidentical inverted repeats by hybridizing fragments from plasmids pEO30HE and pUC8S3B. Only reactions in the pUC8S3B strand are shown. *A*, DNase I and nuclease P1 reactivity. *P* (− or +) indicates control or PARP-1/DNA binding reactions. *GATC*, sequencing markers. The positions of PARP-1-dependent cleavage by DNase I are indicated by the *filled arrowheads*. *B*, sequence positions of PARP-1-dependent cleavage by DNase I and nuclease P1 in the hairpin are indicated by the *filled* and *hollow arrowheads*, respectively.

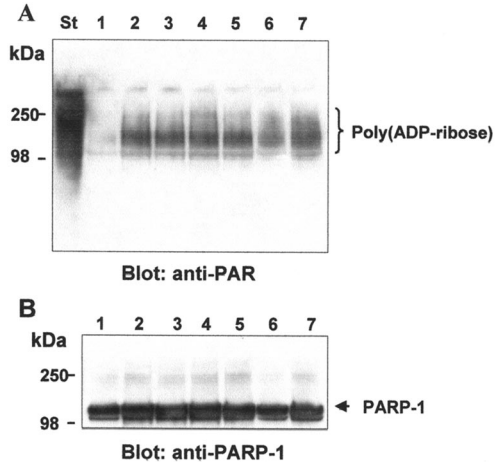

FIG. 5. **Auto-poly(ADP-ribosyl)ation upon structure-specific PARP-1 binding to DNA.** *A*, immunoblot analyses of the *in vitro* ADP-ribose synthesis by human PARP-1 at 450 μM βNAD$^+$ and an 8:1 molar ratio of protein to DNA. The reaction was stimulated by different types of DNA substrates added in equimolar concentration of 1.7 nM as follows. *Lane 1*, end-protected linear dsDNA; *lane 2*, DNA heteroduplex with a 14-nt loop; *lane 3*, heteroduplex with a 10-nt hairpin; *lane 4*, heteroduplex with a cruciform made of 20- and 30-nt palindromic sequences; *lane 5*, heteroduplex with a 15-nt hairpin; *lane 6*, linear dsDNA with one protected end; *lane 7*, sheared genomic DNA. DNA substrates had both ends protected with streptavidin in *lanes 1–5*, one protected end in *lane 6*, and no end protection in *lane 7*. *In vitro* ADP-ribosylated PARP-1 is shown as a standard (*St*). Molecular mass markers (kDa) are indicated on the *left*. *B*, immunodetection of PARP-1 is shown as a reference for quantitative loading of samples.

DNA Hairpins Are Effective Co-activators of Trans-poly-(ADP-ribosylation) of Histone H1—Histone H1 is a major nuclear acceptor of PAR in chromatin, and its post-translational modification by PARP-1 is thought to play an important role in chromatin structural transitions (reviewed in Ref. 10). Therefore, we investigated whether non-B DNA structures whose formation may be driven by unrestrained torsional tension in genomic DNA (15, 16, 31) have the potential to stimulate poly-(ADP-ribosyl)ation of histone H1 in the absence of DNA damage. For this, we measured the kinetics of trans-poly(ADP-ribosylation) by monitoring PAR synthesis on solid phase-immobilized histone H1. Although this reaction requires a high

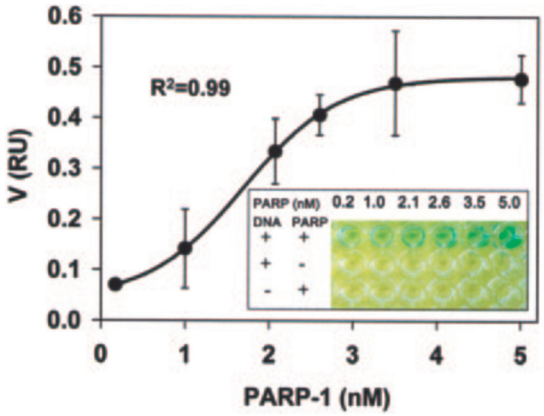

FIG. 6. **Trans-poly(ADP-ribosyl)ation of histone H1 by PARP-1 is stimulated by the three-way junction-containing DNA.** The ADP-ribosylation reaction was carried out in the presence of 450 μM NAD^+, 170 pM end-protected pUC8/pEO30HE heteroduplex, with varying concentrations of PARP-1 (0–5 nM), and histone H1 immobilized on solid phase. Synthesis of ADP-ribose polymers was quantified by a spectroscopic assay as described under "Experimental Procedures," and the reaction rate was expressed in relative units (*RU*) of chromogen absorbance. The *solid line* represents the best fit curve to the equation $Y = 0.49/(1 + \exp(-(x - x_0)/0.68))$ obtained by the nonlinear least squares regression at 99% confidence (R^2) as described under "Experimental Procedures." Each data point is the mean of three independent experiments, and the *error bars* show the standard deviation of the mean. The *inset* shows a representative experiment for the detection of poly(ADP-ribose) attached to histone H1 in the presence of varying concentrations of human PARP-1.

concentration ratio of histone H1 to PARP-1, this model better represents histone incorporation in chromatin than assays of histone modification in solution (25, 32). The co-enzymatic activity of hairpin-containing dsDNA as a function of enzyme concentration was evaluated at a fixed DNA concentration and a saturating NAD^+ concentration (33). In this assay, PARP-1 concentrations were limited to a low nanomolar range, because enzyme concentrations above 20 nM may inhibit ADP-ribose polymerization *in vitro* (33).

Fig. 6 shows that DNA hairpins are effective co-enzymatic activators of the trans-poly(ADP-ribosylation) of histone H1 and that the reaction rate as a function of enzyme concentration increases in a sigmoidal fashion. At subnanomolar PARP-1 concentrations, the rate of PAR accumulation increased slowly. Following a phase of reaction in which the rate accelerated proportional to the amount of enzyme and in an almost linear fashion, the reaction rate leveled off above 4 nM PARP-1 (Fig. 6). This kinetic behavior is typical for allosteric enzymes, many of which are oligomeric, including zinc finger-containing DNA-binding proteins (34). The second order kinetics behavior of the poly(ADP-ribosyl)ation reaction upon PARP-1 binding to the DNA hairpins in the absence of free DNA ends is similar to the sigmoidal kinetics of PAR synthesis stimulated by DNA containing strand breaks (33, 35). The sigmoidal type of enzyme kinetics indicates that the ADP-ribose polymerization reaction requires two molecules of PARP-1 and that PARP-1 likely forms a catalytic dimer on DNA (33, 36). Consistent with this suggestion, PARP-1 dimerization was demonstrated in footprinting experiments upon PARP-1 binding to nicks in dsDNA and to the junction between double-stranded DNA and an overhanging single-stranded DNA (35, 37).

Kinetic Characterization of Trans-poly(ADP-ribosyl)ation Activated by DNA Structure-specific PARP-1 Binding—In aggregate, our observations (Fig. 6) and data from the literature (32, 33, 35, 36) suggest that regardless of the structural type of a DNA co-factor, PARP-1 utilizes a similar mechanism to catalyze poly(ADP-ribosyl)ation. However, the co-enzymatic efficiency of DNA, measured as the rate of poly(ADP-ribosyl)ation, may depend on the structure of the PARP-1-binding site in DNA, which can offer more or less auspicious arrangements to support enzyme cooperativity and its catalytic activation. To test this possibility, we evaluated the co-enzymatic potencies of the distinct types of non-B DNA structures such as loops, hairpins, and cruciforms to stimulate ADP-ribosylation of histone H1. The plots of the histone H1 trans-poly(ADP-ribosyl)ation reaction rates (*V*) *versus* DNA concentration for various DNA constructs are shown in Fig. 7*A*. When both DNA ends were protected in parental B DNA fragments, no activation of the trans-poly(ADP-ribosyl)ation of histone H1 was observed, thus indicating that there was no sequence-specific PARP-1 binding to DNA that might have resulted in PARP-1 activation. Non-B DNA constructs with protected fragment ends stimu-

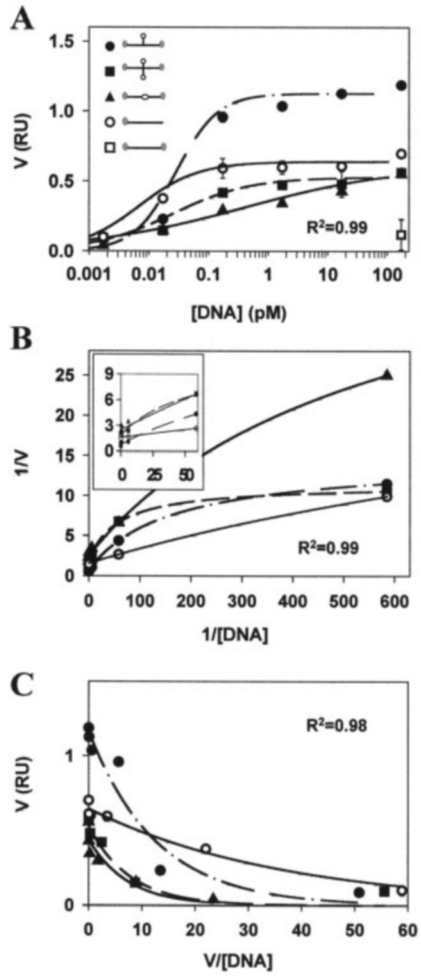

FIG. 7. **Kinetics of trans-poly(ADP-ribosylation) activated by DNA structure-specific PARP-1 binding.** *A*, rates of the trans-poly(ADP-ribosylation) of histone H1 *in vitro* as a function of DNA concentration in the presence of PARP-1 and NAD^+ at fixed concentrations of 8.62 nM and 450 μM, respectively. Histone H1 trans-poly(ADP-ribosylation) was stimulated by end-protected DNA heteroduplexes carrying a 15 bp-hairpin (●), a cruciform (■), and a loop (▲) or linear DNA homoduplexes modified with streptavidin either at one (○) or both DNA ends (□). All of the reactions were performed at 25 °C for 30 min, and the kinetic constants ($K_{0.5}$ and V_{max}) were calculated as described under "Experimental Procedures." The *solid lines* represent the best fit curves obtained by the nonlinear least squares regression at 99% confidence (R^2). The data points are the means of three independent experiments. *B*, Lineweaver-Burk plot of the trans-poly(ADP-ribosylation) reactions stimulated by DNA constructs shown in *A*. The *inset* shows the Lineweaver-Burk plots at the low range of 1/[DNA]. The *solid lines* represent a fit of the data in double-reciprocal plot with R^2 value of 0.99. *C*, nonlinear regression fits of kinetic data to the Eadie-Hofstee plot.

TABLE II

Kinetic constants for PARP-1 activation by a structure-specific binding to DNA

The values for $K_{0.5}$ and V_{max} were obtained from kinetic curves as described under "Experimental Procedures." Relative V_{max} constants (V^{rel}_{max}) for the trans-poly(ADP-ribosylation) reactions were calculated as the ratios of V_{max} for DNA heteroduplexes to V_{max} for blunt end linear dsDNA. The rate constants given are the means from three independent experiments.

DNA duplex	Ends modified	Structural characteristics	$K_{0.5}$	V_{max}	V^{rel}_{max}
			pM		%
pUC8/pEO30HE	two	hairpin	0.028 ± 0.007	1.126 ± 0.043	175.4
pEO30HE/pDT20	two	cruciform	0.024 ± 0.010	0.529 ± 0.038	82.4
pUC8/pMDR1S	two	loop	0.369 ± 0.062	0.618 ± 0.128	96.3
pUC8/pUC8	one	blunt end	0.007 ± 0.002	0.642 ± 0.025	100

lated the reaction at rates comparable with that achieved by linear dsDNA with an unprotected blunt end. The initial rates of all reactions increased as a function of DNA concentration, although their V_{max} were dependent on the structures of the DNA co-factors.

When the trans-poly(ADP-ribosyl)ation reaction rates were plotted in the Lineweaver-Burk coordinates, a marked deviation from linearity was observed. The nonlinear shapes of the plots (Fig. 7*B*) became even more pronounced in the Eadie-Hofstee coordinates (Fig. 7*C*), thus indicating that the reaction curves do not fit the Michaelis-Menten kinetics and thereby cannot be characterized by K_m. Non-Michaelis-Menten kinetics of the trans-poly(ADP-ribosyl)ation reaction indicates that PARP-1 is a regulated (allosteric) enzyme and that non-B DNA structures, such as stably unwound regions, hairpins, and cruciforms, are all highly potent co-enzymatic activators of PARP-1. The kinetic data (Fig. 7*A*) were analyzed by a nonlinear fitting procedure, and the $K_{0.5}$ and V_{max} characteristic constants were determined (Table II). The values of $K_{0.5}$ for different DNA secondary structure co-factors follow the order: cruciform ≤ hairpin ≪ loop. Notably, PARP-1 has almost the same $K_{0.5}$ constants for DNA hairpins and for cruciforms, suggesting a structural similarity of PARP-1 recognition sites in the three- and four-way DNA constructs. This also suggests that the stably extruded stem-loops present a favorable spatial arrangement for PARP-1 binding to undamaged dsDNA. With respect to the maximum reaction velocity, the three-way junction structure exhibited the highest co-enzymatic potency in stimulating the trans-poly(ADP-ribosyl)ation of histone H1 (V_{max} = 1.126) as compared with DNA cruciforms, loops, or DNA blunt ends. These data are in line with the recent observation that damaged DNA exhibited a lower co-enzymatic efficacy than end-protected AT-rich DNA homopolymers (32). The latter have a high propensity to form base unpaired regions, thereby presenting binding sites for PARP-1 in a DNA structure-specific fashion.

Although DNA hairpins, cruciforms, and loops have different co-enzymatic efficiencies, they exhibited common kinetic behavior (Fig. 7*A*). That is, the synthesis of poly(ADP-ribose) was stimulated by very low (picomolar) DNA concentrations, and the reactions reached steady-state rates over a narrow range of DNA concentration (0–0.1 pM). A sharp transition of the reaction rates from states of low to high enzyme activity suggests that the non-B DNA co-factors regulate PARP-1 function in an "on-off" fashion. Further investigations of the mode(s) of PARP-1 binding to DNA strand breaks and to undamaged DNA in a structure-specific fashion are required to understand the nature of the factors influencing the efficiency of PARP-1 activation upon DNA binding.

Functional Significance of PARP-1 Binding to Non-B DNA Structures—Our data demonstrate that non-B DNA structures, such as hairpins, cruciforms, and loops exhibit high co-enzymatic potency in stimulating poly(ADP-ribosyl)ation and that the structural features of different DNA co-factors are important for the kinetics of PARP-1 catalysis activated by undamaged DNA. It is possible that different types of DNA structure represent unequally favorable binding sites for PARP-1 molecules to form catalytically active DNA-protein complexes. This, in turn, would influence the kinetic parameters of PARP-1 activation in chromatin and may explain variations in co-enzymatic activity of different types of DNA co-factors, such as various DNA strand breaks (38) or non-B DNA structures (Table II).

Following genotoxic stress, PARP-1 activation by DNA strand breaks leads to ADP-ribosylation of nuclear proteins and chromatin loosening, thus facilitating DNA damage repair at multiple sites randomly distributed throughout the genome. In contrast to the genotoxic insult, physiological chromatin modification must occur locally and be well timed to ensure transient changes in genome operation at certain sites in chromatin. Our data provide a mechanistic basis for the physiological function of PARP-1 in the dynamics of the local modulation of chromatin structure. PARP-1 activation upon binding to base-unpaired regions and stem-loops structures in DNA leads to a local PAR modification of histones and non-histone proteins at genomic sites where such DNA structures are formed. Subsequent PARP-1 auto-modification results in its dissociation from DNA leading to an enzymatic self-inactivation (39), thus ensuring a transient character of chromatin ADP-ribosylation. In combination with the PAR-glycohydrolase degradation of ADP-ribose polymers on acceptor proteins (40), PARP-1 interaction with DNA secondary structures provides a mechanism for local and transient chromatin modification by PAR during physiological nuclear processes.

Acknowledgments—Authors thank Drs. A. Eliseev, V. Movsesyan, and L. Zoubak for providing assistance with software and data base analyses and Alex Gamero for helping to develop the heteroduplex purification procedure. We also thank Drs. A. Dritschilo, R. Sinden, and S. Fuchs for valuable discussions and critical suggestions and V. Forrester for manuscript proofreading.

REFERENCES

1. Ame, J. C., Spenlehauer, C., and de Murcia, G. (2004) *Bioessays* **26,** 882–893
2. Althaus, F. R., and Richter, C. (1987) *Mol. Biol. Biochem. Biophys.* **37,** 1–237
3. Benjamin, R. C., and Gill, D. M. (1980) *J. Biol. Chem.* **255,** 10493–10501
4. D'Amours, D., Desnoyers, S., D'Silva, I., and Poirier, G. G. (1999) *Biochem. J.* **342,** 249–268
5. Satoh, M. S., and Lindahl, T. (1992) *Nature* **356,** 356–358
6. Nicholson, D. W., Ali, A., Thornberry, N. A., Vaillancourt, J. P., Ding, C. K., Gallant, M., Gareau, Y., Griffin, P. R., Labelle, M., Lazebnik, Y. A., Munday, N. A., Raju, S. M., Smulson, M. E., Yamin, T. T., Yu, V. L., and Miller, D. K. (1995) *Nature* **376,** 37–43
7. Berger, N. A. (1985) *Radiat. Res.* **101,** 4–15
8. de Murcia, G., Huletsky, A., Lamarre, D., Gaudreau, A., Pouyet, J., Daune, M., and Poirier, G. G. (1986) *J. Biol. Chem.* **261,** 7011–7017
9. Realini, C., and Althaus, F. R. (1992) *J. Biol. Chem.* **267,** 18858–18865
10. Rouleau, M., Aubin, R. A., and Poirier, G. G. (2004) *J. Cell Sci.* **117,** 815–825
11. Tulin, A., and Spradling, A. (2003) *Science* **299,** 560–562
12. Yu, W., Ginjala, V., Pant, V., Chernukhin, I., Whitehead, J., Docquier, F., Farrar, D., Tavoosidana, G., Mukhopadhyay, R., Kanduri, C., Oshimura, M., Feinberg, A. P., Lobanenkov, V., Klenova, E., and Ohlsson, R. (2004) *Nat. Genet.* **36,** 1105–1110
13. Kraus, W. L., and Lis, J. T. (2003) *Cell* **113,** 677–683
14. Soldatenkov, V. A., and Potaman, V. N. (2004) *Curr. Drug Targets* **5,** 357–365
15. Leonard, M. W., and Patient, R. K. (1991) *Mol. Cell. Biol.* **11,** 6128–6138

16. Ljungman, M., and Hanawalt, P. C. (1992) *Proc. Natl. Acad. Sci. U. S. A.* **89,** 6055–6059
17. Ackerman, S. L., Minden, A. G., and Yeung, C. Y. (1993) *Proc. Natl. Acad. Sci. U. S. A.* **90,** 11865–11869
18. Gradwohl, G., Mazen, A., and de Murcia, G. (1987) *Biochem. Biophys. Res. Commun.* **148,** 913–919
19. Sastry, S. S., and Kun, E. (1990) *Biochem. Biophys. Res. Commun.* **167,** 842–847
20. Oei, S. L., Herzog, H., Hirsch-Kauffmann, M., Schneider, R., Auer, B., and Schweiger, M. (1994) *Mol. Cell. Biochem.* **138,** 99–104
21. Galande, S., and Kohwi-Shigematsu, T. (1999) *J. Biol. Chem.* **274,** 20521–20528
22. Soldatenkov, V. A., Chasovskikh, S., Potaman, V. N., Trofimova, I., Smulson, M. E., and Dritschilo, A. (2002) *J. Biol. Chem.* **277,** 665–670
23. Oussatcheva, E. A., Shlyakhtenko, L. S., Glass, R., Sinden, R. R., Lyubchenko, Y. L., and Potaman, V. N. (1999) *J. Mol. Biol.* **292,** 75–86
24. Shlyakhtenko, L. S., Potaman, V. N., Sinden, R. R., Gall, A. A., and Lyubchenko, Y. L. (2000) *Nucleic Acids Res.* **28,** 3472–3477
25. Kun, E., Kirsten, E., and Ordahl, C. P. (2002) *J. Biol. Chem.* **277,** 39066–39069
26. Sinden, R. R. (1994) *DNA Structure and Function,* pp. 138–139, Academic Press, San Diego, CA
27. Yoo, S., Kimzey, A., and Dynan, W. S. (1999) *J. Biol. Chem.* **274,** 20034–20039
28. Zhang, Z., Hildebrandt, E. F., Simbulan-Rosenthal, C. M., and Anderson, M. G. (2002) *Virology* **296,** 107–116
29. Gaal, J. C., and Pearson, C. K. (1985) *Biochem. J.* **230,** 1–18
30. Loetscher, P., Alvarez-Gonzalez, R., and Althaus, F. R. (1987) *Proc. Natl. Acad. Sci. U. S. A.* **84,** 1286–1289
31. Kramer, P. R., Fragoso, G., Pennie, W., Htun, H., Hager, G. L., and Sinden R. R. (1999) *J. Biol. Chem.* **274,** 28590–28597
32. Kun, E., Kirsten, E., Mendeleyev, J., and Ordahl, C. P. (2004) *Biochemistry* **43,** 210–216
33. Mendoza-Alvarez, H., and Alvarez-Gonzalez, R. (1993) *J. Biol. Chem.* **268,** 22575–22580
34. Pomerantz, J. L., Wolfe, S. A., and Pabo, C. O. (1998) *Biochemistry* **37,** 965–970
35. Pion, E., Bombarda, E., Stiegler, P., Ullmann, G. M., Mely, Y, de Murcia, G., and Gerard, D. (2003) *Biochemistry* **42,** 12409–12417
36. Bauer, P. I., Buki, K. G., Hakam, A., and Kun, E. (1990) *Biochem. J.* **270,** 17–26
37. Gradwohl, G., Menissier de Murcia, J. M., Molinete, M., Simonin, F., Koken, M., Hoeijmakers, J. H., and de Murcia, G. (1990) *Proc. Natl. Acad. Sci. U. S. A.* **87,** 2990–2994
38. D'Silva, I., Pelletier, J. D., Lagueux, J., D'Amours, D., Chaudhry, M. A., Weinfeld, M., Lees-Miller, S. P., and Poirier, G. G. (1999) *Biochim. Biophys. Acta.* **1430,** 119–126
39. Ferro, A. M., and Olivera, B. M. (1982) *J. Biol. Chem.* **257,** 7808–7813
40. Desnoyers, S., Shah, G. M., Brochu, G., Hoflack, J. C., Verreault, A., and Poirier, G. G. (1995) *Biochimie* (*Paris*) **77,** 433–438